IJE TRANSACTIONS B: Applications Vol. 35, No. 02, (February 2022) 481-492

International Journal of Engineering

Journal Homepage: www.ije.ir

Experimental Study on Surface Integrity of Ti6Al4V by Broaching

P. Khanjanzadeh[a], H. Amirabadi*[b], J. Sadri[c,d]

[a] *Department of Mechanical Engineering, University of Birjand, Birjand, Iran*
[b] *Faculty of Engineering, University of Neyshabur, Neyshabur, Iran*
[c] *Department of Computer Science & Software Engineering, Concordia University, Montreal, Canada*
[d] *Camp in Labs Foundation, 1 Westmount Square, Bureau 1001, Westmount, Quebec, Canada*

PAPER INFO

Paper history:
Received 30 September 2021
Received in revised form 14 November 2021
Accepted 02 December 2021

Keywords:
Broaching Tool
Cutting Tool Design
Residual Stress
Titanium Alloy

ABSTRACT

The performance of many parts in the airplane, aircraft engine and biomedical implants is highly related to their fatigue life, which is clearly depend on the condition of their surface integrity. The geometry parameters of broaching tools have an important influence on the surface integrity after broaching Ti6Al4V alloy. Therefore, this research studies the surface integrity of Ti6Al4V by broaching. The surface integrity is studied at different geometric parameters such as rake angles (α, and α_0), clearance angles (β, and β_0), and radius of the cutting edge (r_0) in two last teeth of the broaching tool that perform chipping. The broached surface integrity is assessed in cases of surface roughness, microstructural, residual stresses, and micro hardness. These results show that the sample broached by tool number 1 ($\alpha = 18.4, \beta = 3.1, \alpha_0 = 45, \beta_0 = 9, r_0 = 0.02$) had higher surface integrity because it was the smoothest surface and the thinnest deformed layer among the other samples. Since the main criterions in selection of the optimal tool are to create the smoothest surface and the least deformed layer depth in the broached sample, tool number 1($\alpha = 18.4, \beta = 3.1, \alpha_0 = 45, \beta_0 = 9, r_0 = 0.02$) is suggested as the optimal tool.

doi: *10.5829/ije.2022.35.02b.24*

1. INTRODUCTION

Broaching is a machining process widely used to produce some aspects because of the surface integrity state and high dimensional quality. Therefore, the surface integrity feature gained in broaching is very important in increasing the life of fatigue [1]. The Ti6Al4V alloy is extensively used in aircraft engine and medical implants which high fatigue life and corrosion resistance are needed [2, 3]. Considering the working conditions of the turbine blade such as the presence of high centrifugal forces, and high temperatures during operation, the design of the broaching tool that creates the minimum residual stress on it is required [4].

Surface integrity is inherent or enhanced condition of a surface produced in machining or other surface generation operation [5]. Surface integrity states the performance and the quality of a machined part and contains of the metallurgical conditions (microstructure, phase transformation, etc.), mechanical properties (micro hardness, residual stresses, etc.), and surface roughness [6]. In most cases, to prevent early failure and fatigue of the parts, the smoothest surface finish is desirable [7]. After any thermos-mechanical manufacturing operation such as machining processes, different features of surface integrity are affected [8].

Here, a history of research performed in the area of surface integrity of alloys by machining, has been presented. He and Zhang [9] investigated the influences of cutting factors on the surface integrity of broached TC9 alloy. Schulze et al. [10] used FE simulation to estimate created residual stress on the broached surface of SAE 5120 alloy. Kong et al. [11] studied the influences of cutting factors on saw-toothed chip formation of nickel-base alloy GH4169, using FE simulation. Jafarian et al. [12, 13] developed a robust method to predict and improve surface residual stress in the turning operation of Inconel718. Ortize-de-Zarate et al. [14] presented an experimental and FE method analysis of surface integrity of broached Ti6Al4V. They studied the effect of cutting

*Corresponding Author Institutional Email: hamirabadi@neyshabur.ac.ir (H. Amirabadi)

Please cite this article as: P. Khanjanzadeh, H. Amirabadi, J. Sadri, Experimental Study on Surface Integrity of Ti6Al4V by Broaching, ***International Journal of Engineering, Transactions B: Applications***, Vol. 35, No. 2, (2021) 481-492

speed on cutting forces, chip morphology and surface integrity of broached Ti6Al4V. Kaway and Zhang [15] investigated surface integrity of Ti6Al4V in ball end milling process. Childs et al. [16] proposed a model that employs a failure criterion as a function of stress and temperature for Ti6AlV4. Bertolini et al. [17] evaluated the EBM Ti6Al4V machinability in terms of the relationship between the surface integrity with corrosion resistance and fatigue life. Khanjanzadeh et al. [18] proposed the optimal geometry for a broaching tool by using FE simulation which generates the lowest residual stress in the broached surface of the Ti6Al4V alloy. The mentioned studies showed that so far, relatively little study into surface integrity of Ti6Al4V by broaching has been done.

The main contribution of this manuscript is that for the first time, the experimental study is performed about the effect of broaching tool geometry on the surface integrity of Ti6Al4V. In our previous paper [18], based on finite element simulation and optimization using a genetic algorithm, it was shown that the optimal geometric parameters of the last two teeth of the broaching tool that perform chipping, depend on the percentage of effect of each of the temperature and effective strain factors.

2. MATERIALS AND METHODS

Figure 1 indicates the block diagram of the research method. In this research, based on the results of the Pareto diagram obtained in our previous paper [18], five tools with different optimal geometric characteristics were fabricated. Then the surface integrity of the broached samples was experimentally compared. Finally, the geometric parameters of the optimal broaching tool were introduced.

2. 1. Materials The test material is the grade 5 of Ti6Al4V. The wrought material was supplied in form of plates of 75mm × 25mm × 9mm and annealed at 955℃ for one hour. Table 1 summarized the chemical composition of the material. The mechanical properties of the material are listed in Table 2. The final specimens were produced using the wire cut machine. Then the samples were mounted on a fixture. The test workpieces are indicated in Figure 2.

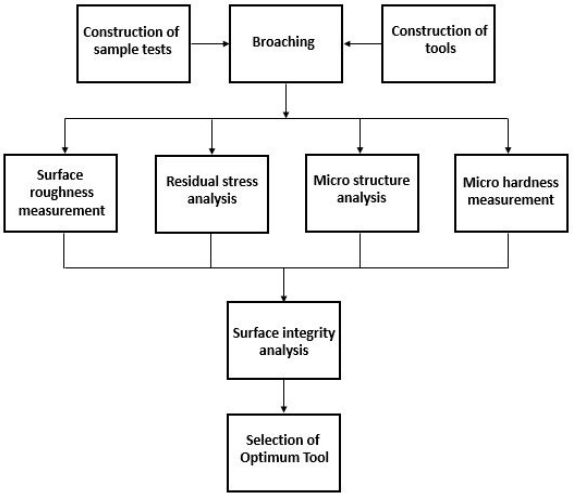

Figure 1. Block diagram of the research method

2. 2. Broaching Tests In our previous work [18], based on finite element simulation and optimization using a genetic algorithm, it was shown that the optimal geometric parameters of the last two teeth of the broaching tool that perform chipping, depend on the percentage of effect of the temperature and effective strain factors. In this study, based on the results of the Pareto diagram obtained in our previous research, five tools with different optimal geometric characteristics were constructed. Table 3 and Figure 3 show the geometric specifications of broaching tools based on our previous research work [18].

The broaching tools were made of a WC blade by a Robofil Charmilles wire cut machine. Thus, in total five tools were made. The cutting tools were mounted on a tool holder. The cutting speed of broaching operations was 3 m/min. Experimental tests were performed on an OKK PCV-55 3Axis CNC machine, 48"×22". Figure 4 shows the broaching setup. Three repetitions were done for each cutting condition. So in total, fifteen tests were carried out.

TABLE 1. Chemical composition of Ti6Al4V

Element	Ti	Al	V	Fe	Nb	Cr	Sn	Si	Mo	W	Mn	Cu	Zr
Mass%	Base	5.65	4.52	0.18	0.012	0.011	<0.03	0.006	<0.01	<0.02	<005	<0.005	<0.002

TABLE 2. Mechanical properties of annealed Ti6Al4V [19]

Yield stress (MPa)	Ultimate stress (MPa)	Young's Module (GPa)	Micro hardness (HV)	Poisson's ratio
880	950	113.8	350	0.342

a b

Figure 2. Test workpiece a) workpiece drawing, b) The workpieces mounted on the fixture

TABLE 3. Geometric dimensions of tools (α: Rake angle of the first tooth, β: Clearance angle of the first tooth, α_0: Rake angle of the second tooth, β_0: Clearance angle of the second tooth, r_1: The radius of curvature of the gullet behind of the first tooth, r_2: The radius of curvature of the gullet behind of the second tooth)

Tool's No.	α	β	α_0	β_0	r_0 (mm)	r_1 (mm)	r_2 (mm)
1	18.4^0	3.1^0	45^0	9^0	0.02	3.62	4.87
2	18.4^0	3.1^0	45^0	9^0	0.01	3.62	4.87
3	18.4^0	3.1^0	35^0	9^0	0.01	3.62	4.35
4	18.4^0	3.1^0	35.4^0	8.2^0	0.01	3.62	4.35
5	18.4^0	3.1^0	35^0	8.4^0	0.01	3.62	4.34

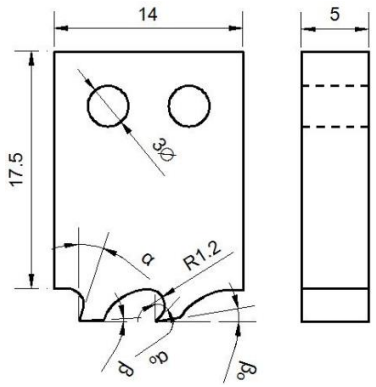

Figure 3. Broaching tool's drawing. (α: Rake angle of the first tooth, β: Clearance angle of the first tooth, α_0: Rake angle of the second tooth, β_0: Clearance angle of the second tooth, R: radius of the internal curvature of the gullet

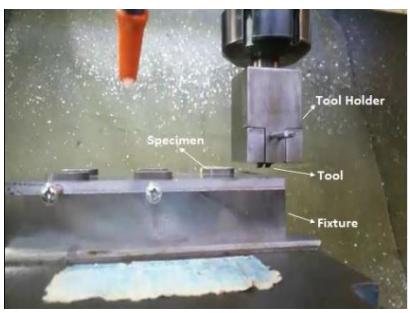

Figure 4. Broaching setup

2. 3. 1. Surface Roughness Analyze The surface roughness is measured at the center of each broached slot along the cutting direction using the contact method. Surface roughness measurements were done with a portable profilometer INNOVATEST® Model TR200 equipment. Table 4 indicates the conditions of surface roughness tests.

2. 3. 2. Residual Stresses Analyze The residual stresses were measured at the center of each broached slot using the X-Ray Diffraction (XRD) method via the sin2ψ technique. Measurements of residual stress were performed with a HAOYUAN Model DX-2700BH. Tilting was done along the cutting direction. Poisson's ratio was assumed to be 0.342 and Young modulus 113.8 Gpa [19].

2. 3. 3. Microstructural Images Analyze Grinding of the Ti6Al4V samples were done using up to 2000 SiC

TABLE 4. Surface roughness measurement parameters

Cutoff	0.8 mm
Tracing length	4 mm
Radius of the probe tip	0.05 μm
Tracing speed	0.5 mm/s
Resolution	0.005 μm

grit paper. Then the samples polished by 3µm Al_2O_3 colloidal dispersion in distilled water. Finally, the polished samples were rinsed in distilled water and dried by a heater. To observe the microstructure of the samples, it is necessary to do chemical etching of the samples. Therefore, the specimens were reacted with an etchant (85% H_2O, 10%HF and 5%HNO_3) for 5 seconds. Then etched samples were washed in distilled water and then dried by a heater. The microstructure images were prepared by a UNION optical microscope and an scanning electron microscope Model JEOL840.

2. 3. 4. Micro Hardness Analyze Measurements of micro hardness were carried out using the Micromet 1 Buhler tester. The micro hardness test conditions are given in Table 5. Measurements were done on the middle line of the polished section surface of each. Indentations were made along a line consisted by six points, beginning the depth of 50 µm from the broached surface. The distance between two successive points kept enough to avoid measurement errors.

3. RESULTS AND DISCUSSION

3. 1. Surface Roughness The results of surface roughness measurements of the broached specimens are summarized in Table 6. As shown in Figures 5-7, the results of measuring the surface roughness of the broached specimens indicate that with an increase in r_0 (radius of the cutting edge of the second tooth) from 0.01 mm to 0.02 mm, the R_a and R_z of the broached surface decrease from 0.232 µm and 0.330 µm to 0.162 µm and 0.316 µm, respectively. An increase in the radius of the cutting edge reduces the penetration of the tool into the workpiece. As a result, the surface roughness is decreased. Also, with an increase in α_0 (second tooth rake angle) from 35 degrees to 45 degrees, the R_a and R_z of

TABLE 5. The micro hardness test conditions

Indenter	Force	Loading time
Diamond pyramid	100 grf	15 s

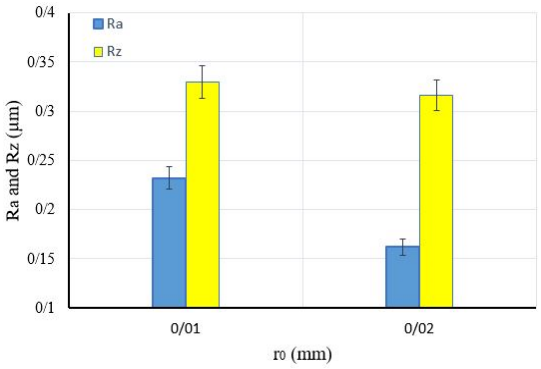

Figure 5. Effect of radius of cutting edge (r_0) on R_a and R_z

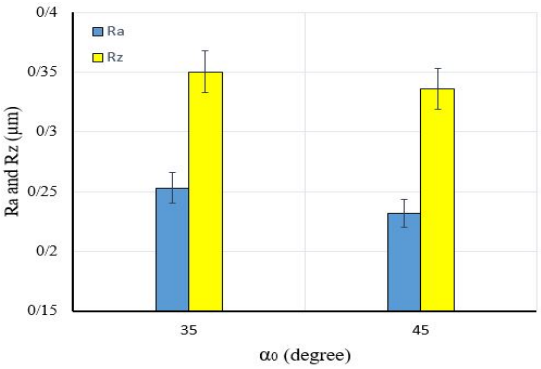

Figure 6. Effect of rake angle of the second tooth (α_0) on R_a and R_z

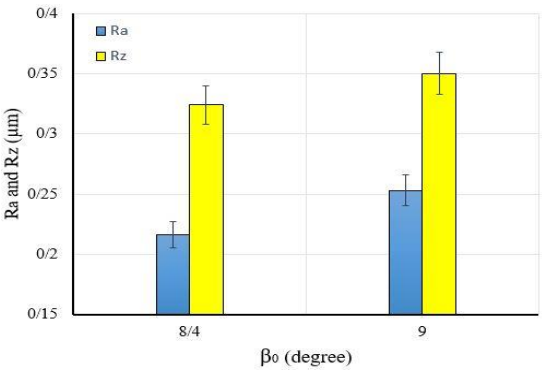

Figure 7. Effect of clearance angle of the second tooth (β_0) on R_a and R_z

TABLE 6. Surface roughness of specimens

Tool's No.	α	β	α_0	β_0	r_0 (mm)	Ra (µm)	Rz (µm)
1	18.4^0	3.1^0	45^0	9^0	0.02	0.162	0.316
2	18.4^0	3.1^0	45^0	9^0	0.01	0.232	0.330
3	18.4^0	3.1^0	35^0	9^0	0.01	0.253	0.350
4	18.4^0	3.1^0	35.4^0	8.2^0	0.01	0.342	0.387
5	18.4^0	3.1^0	35^0	8.4^0	0.01	0.216	0.324

the broached surface decrease from 0.253 µm and 350 µm to 0.232 µm and 0.336 µm, respectively. The cause of these changes can be found according Merchant circle (Figure 8) and Equations (1) and (2) in mechanic of orthogonal cutting [20].

$$F_c = \frac{tb\tau\cos(\beta-\alpha_0)}{\sin\emptyset\cos(\emptyset+\beta-\alpha_0)} \quad (1)$$

$$F_t = \frac{tb\tau\sin(\beta-\alpha_0)}{\sin\emptyset\cos(\emptyset+\beta-\alpha_0)} \quad (2)$$

where F_c is the cutting force, t is the thickness of chip before cutting, b is the cutting width, τ is the yield shear stress, β is the friction angle, α_0 is the rake angle, ϕ is the shear angle, and F_t is the thrust force [20]. Increasing α_0 reduces the thrust force and as a result, the surface roughness is decreased.

Moreover, with an increase in β_0 (clearance angle of the second tooth) from 8.4 degrees to 9 degrees, the R_a and R_z of the broached surface increase from 0.216 µm and 0.324 µm to 0.253 µm and 0.350 µm, respectively. Increasing β_0 reduces the contact of the tool with the workpiece surface. As a result, the surface roughness has increased.

3. 2. Residual Stresses The results of residual stress measurements of the broached specimens are shown in Table 7. In all cases, the residual stresses are compressive.

As shown in Figures 9-11, the results of measuring the residual stress of the broached specimens indicate that

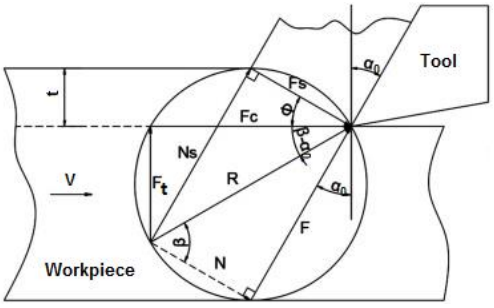

Figure 8. Merchant circle. F_c is the cutting force, t is the thickness of chip before cutting, β is the friction angle, α_0 is the rake angle, ϕ is the shear angle, and F_t is the thrust force [20].

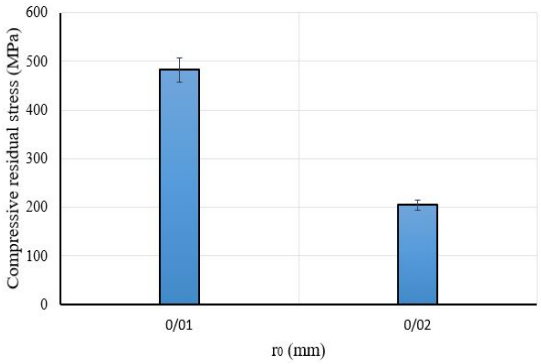

Figure 9. Effect of radius of the cutting edge (r_0) on residual stress

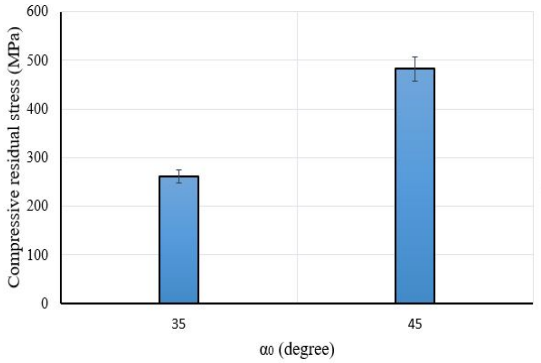

Figure 10. Effect of rake angle of the second tooth (α_0) on residual stress

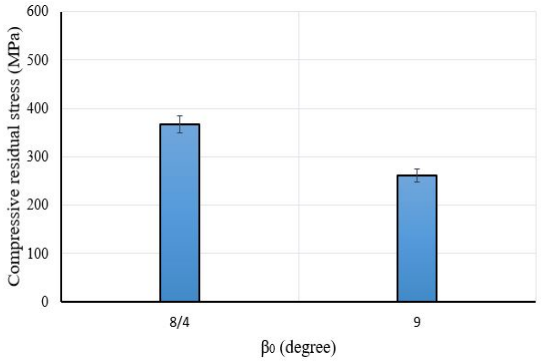

Figure 11. Effect of clearance angle of the second tooth (β_0) on residual stress

TABLE 7. Compressive residual stresses of specimens

Tool's No.	α	β	α_0	β_0	r_0 (mm)	Residual stress (MPa)
1	18.4^0	3.1^0	45^0	9^0	0.02	205
2	18.4^0	3.1^0	45^0	9^0	0.01	482
3	18.4^0	3.1^0	35^0	9^0	0.01	261
4	18.4^0	3.1^0	35.4^0	8.2^0	0.01	202
5	18.4^0	3.1^0	35^0	8.4^0	0.01	367

increasing r_0 (radius of the cutting edge of the second tooth) from 0.01 mm to 0.02 mm, causes a considerable decrease in the compressive residual stress created in the workpiece from 482 MPa to 205 MPa. Increasing the radius of the cutting edge reduces the penetration of the tool into the workpiece. As a result, reduces the residual stress created in broached surface.

Also, with increasing α_0 (rake angle of the second tooth) from 35 degrees to 45 degrees, the compressive residual stress created in the workpiece increases from 261 MPa to 482 MPa. Increasing α_0 increases the cutting force. As a result, the residual stress created in broached surface is increased. Moreover, with increasing β_0 (clearance angle of the second tooth) from 8.4 degrees to 9 degrees, the compressive residual stress created in the workpiece decreased from 367 MPa to 261 MPa. Increasing β_0 reduces the contact of the tool with the workpiece surface. As a result, the residual stress created in broached surface decreased.

3. 3. Microstructural Analysis Titanium alloys are classified according to the phases in their structure. Ti6Al4V alloy is the most important and widely used α+β titanium alloy. Aluminum and vanadium alloy elements are stabilizer of the alpha and beta phases, respectively. Figure 12 shows the phase diagram of Ti6Al4V [19]. Figure 13 depicts the microstructure of annealed material which contains a mixed α + β coaxial phase structure. The structure consists of α-shaped plates (light) and inter granular beta (dark). Figures 14-18 show the microstructure of the surface perpendicular to the broached surface of the test specimens.

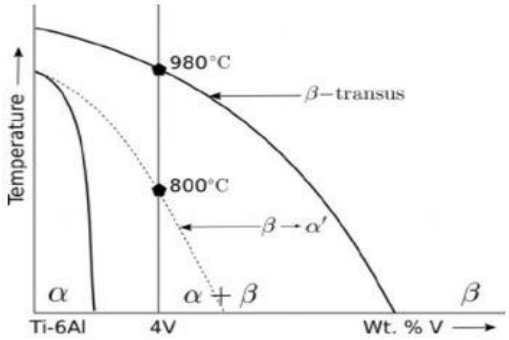

Figure 12. Phase diagram of Ti6Al4V [19]

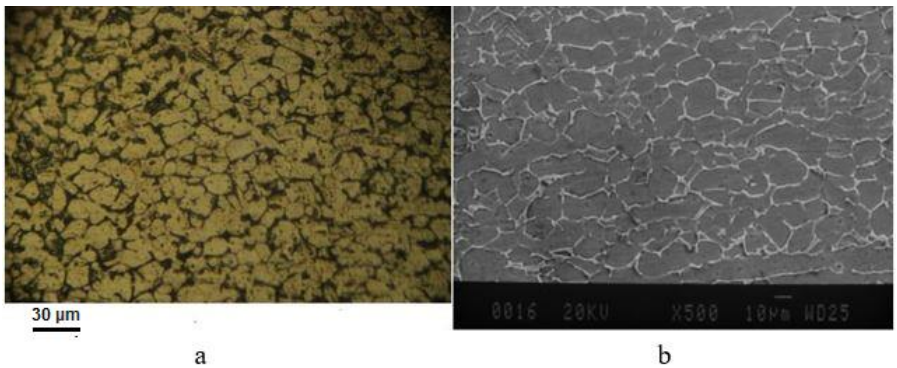

Figure 13. Microstructure of annealed Ti6Al4V (Etching solution: HF10%, HNO_3 5%, H_2O 85%). a) Imaging by optic microscope. The structure consists of α-shaped plates (light) and inter granular beta (dark). b) Imaging by scanning electron microscope (SEM). The structure consists of α-shaped plates (dark) and inter granular beta (light)

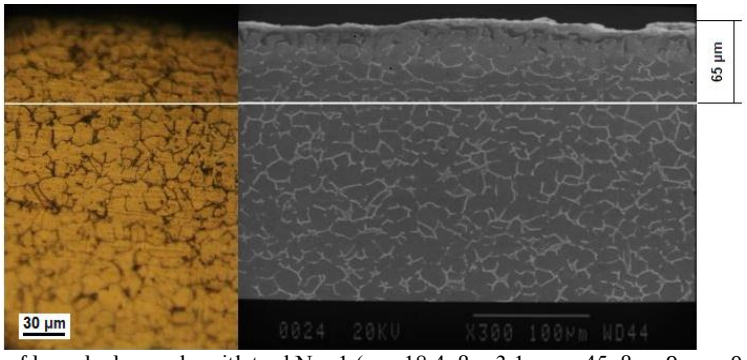

Figure 14. Microstructure of broached sample with tool No. 1 (α = 18.4, β = 3.1, α_0 = 45, β_0 = 9, r_0 = 0.02). The structure consists of α-shaped plates (light) and inter granular beta (dark). (Etching solution: HF10%, HNO_3 5%, H_2O 85%)

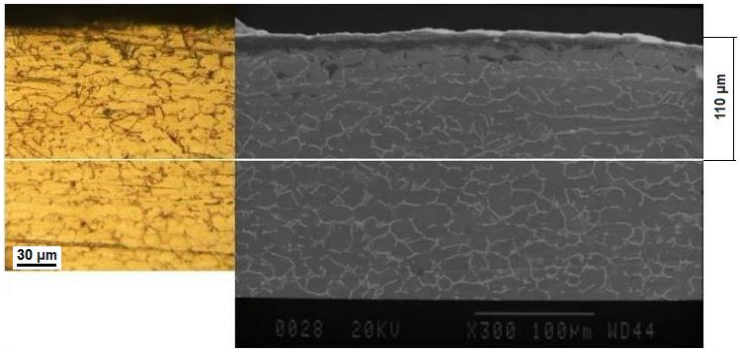

Figure 15. Microstructure of broached sample with tool No. 2 ($\alpha = 18.4$, $\beta = 3.1$, $\alpha_0 = 45$, $\beta_0 = 9$, $r_0 = 0.01$). The structure consists of α-shaped plates (light) and inter granular beta (dark). (Etching solution: HF10%, HNO_3 5%, H_2O 85%)

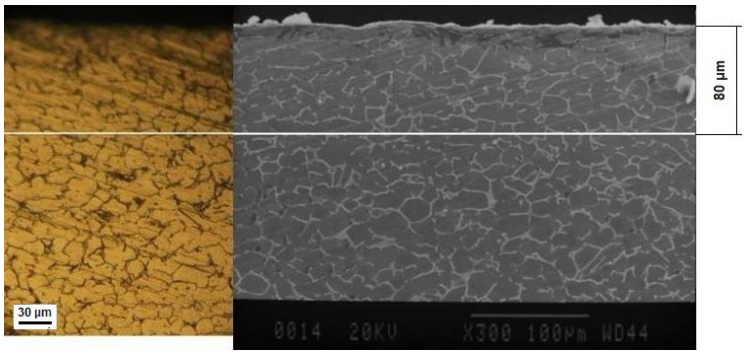

Figure 16. Microstructure of broached sample with tool No. 3 ($\alpha = 18.4$, $\beta = 3.1$, $\alpha_0 = 35$, $\beta_0 = 9$, $r_0 = 0.01$). The structure consists of α-shaped plates (light) and inter granular beta (dark). (Etching solution: HF10%, HNO_3 5%, H_2O 85%)

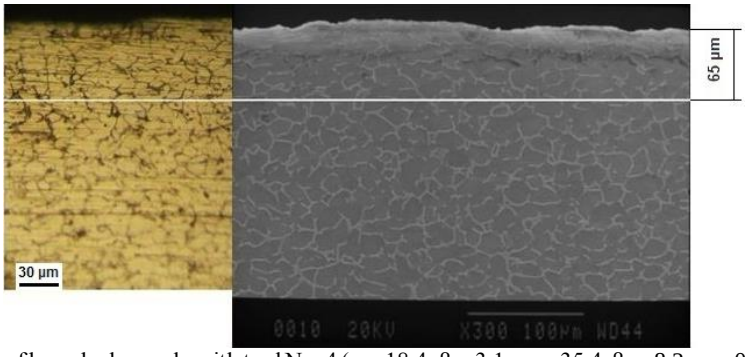

Figure 17. Microstructure of broached sample with tool No. 4 ($\alpha = 18.4$, $\beta = 3.1$, $\alpha_0 = 35.4$, $\beta_0 = 8.2$, $r_0 = 0.01$). The structure consists of α-shaped plates (light) and inter granular beta (dark). (Etching solution: HF10%, HNO_3 5%, H_2O 85%)

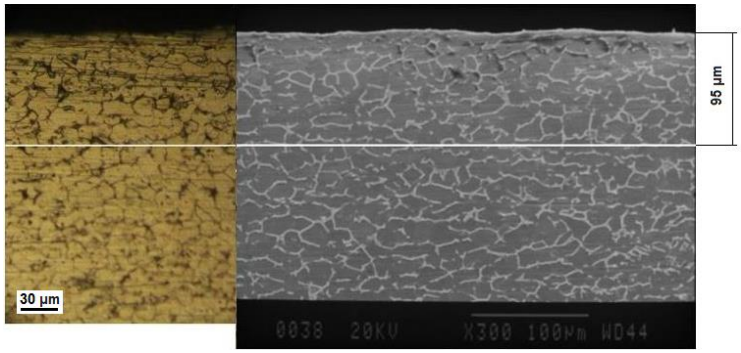

Figure 18. Microstructure of broached sample with tool No. 5 ($\alpha = 18.4$, $\beta = 3.1$, $\alpha_0 = 35$, $\beta_0 = 8.4$, $r_0 = 0.01$). The structure consists of α-shaped plates (light) and inter granular beta (dark). (Etching solution: HF10%, HNO_3 5%, H_2O 85%)

TABLE 8. The depth of deformed layer of broached specimens

Tool's No.	α	β	α_0	β_0	r_0 (mm)	Depth of deformed layer (μm)
1	18.4^0	3.1^0	45^0	9^0	0.02	65
2	18.4^0	3.1^0	45^0	9^0	0.01	110
3	18.4^0	3.1^0	35^0	9^0	0.01	80
4	18.4^0	3.1^0	35.4^0	8.2^0	0.01	65
5	18.4^0	3.1^0	35^0	8.4^0	0.01	95

As shown in Figures 14-18, in the thin layer below the broached surface, the grains are deformed perpendicular to the cutting direction. Comparing the microstructure of the broached specimens with the annealed specimen, despite the plastic deformation, no phase transformation can be detected; because of the cutting temperature is less than 800°C [18]. Table 8 summarized the results of the depth of deformed layer of broached specimens.

According to the Figures 19-21, the results of microstructural images of the broached specimens show that increasing r_0 (radius of the cutting edge of the second tooth) from 0.01 mm to 0.02 mm, causes a considerable decrease in the depth of the deformed layer in the broached specimen from 110 μm to 65 μm. Increasing the radius of the cutting edge reduces the penetration of the tool into the workpiece. As a result, the depth of the deformed layer reduced.

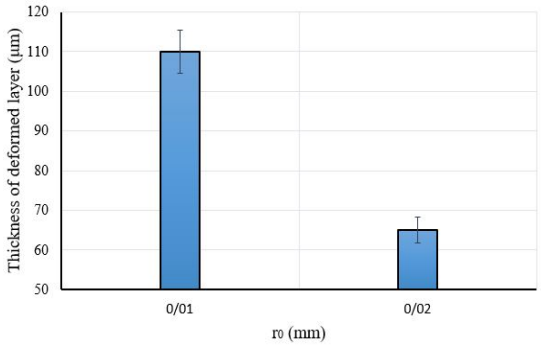

Figure 19. Effect of radius of the cutting edge (r_0) on the depth of the deformed layer

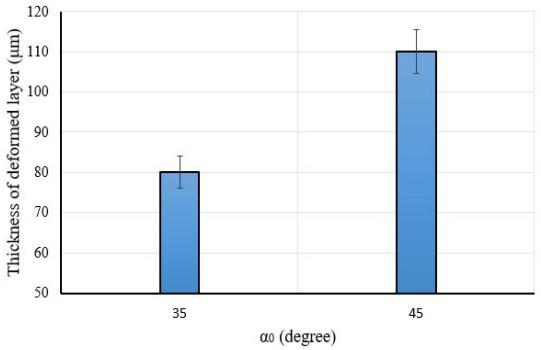

Figure 20. Effect of rake angle of the second tooth (α_0) on the depth of the deformed layer

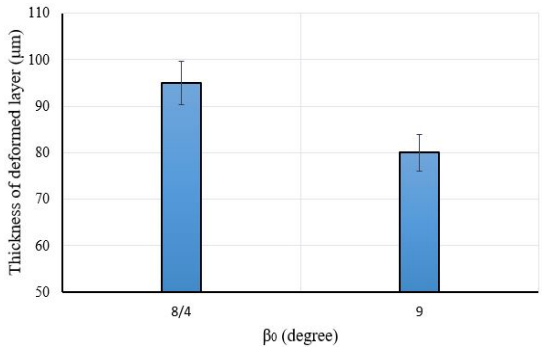

Figure 21. Effect of clearance angle of the second tooth (β_0) on the depth of the deformed layer

Also, with increasing α_0 (rake angle of the second tooth) from 35 degrees to 45 degrees, the depth of the deformed layer in the broached sample increases from 80 μm to 110 μm. Increasing α_0 increases the cutting force. As a result, the depth of the deformed layer is increased. Moreover, by increasing β_0 (clearance angle of the second tooth) from 8.4 degrees to 9 degrees, the depth of the deformed layer in the broached sample decreases from 95 μm to 80 μm. Increasing β_0 reduces the contact of the tool with the workpiece surface. As a result, the depth of deformed in workpiece decreased.

3. 4. Micro Hardness Profiles Figure 22 shows the effect of the geometric parameters of the tool on the micro hardness profiles of the broached specimens. These results show that the micro hardness of the samples increases at the broached surface and gradually decreases with an increase in the distance from the surface. Table 9 shows the maximum micro hardness of broached specimens.

According to Figures 23-25, the micro hardness measurement results of the broached workpieces show that increasing r_0 (radius of the cutting edge of the second tooth) from 0.01 mm to 0.02 mm, decreases the maximum micro hardness created in the workpiece from 401 Vickers to 380 Vickers. Increasing the radius of the cutting edge reduces the penetration of the tool into the

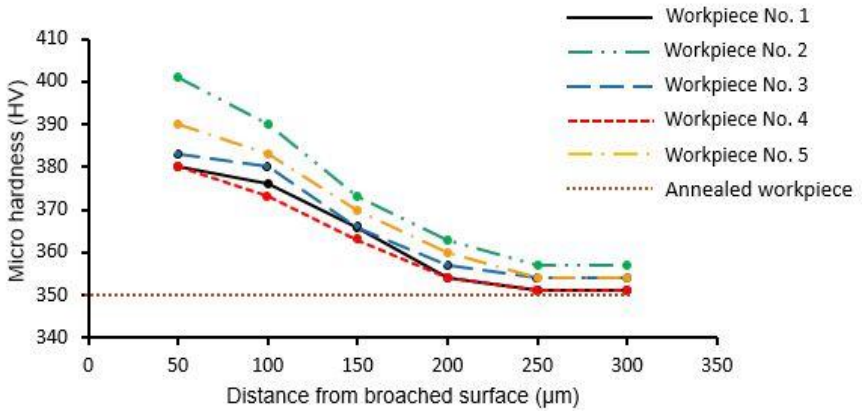

Figure 22. The micro hardness profiles of the broached samples

TABLE 9. The maximum micro hardness of workpieces

Tool's No.	α	β	α_0	β_0	r_0(mm)	Maximum micro hardness (HV)
1	18.4^0	3.1^0	45^0	9^0	0.02	380
2	18.4^0	3.1^0	45^0	9^0	0.01	401
3	18.4^0	3.1^0	35^0	9^0	0.01	383
4	18.4^0	3.1^0	35.4^0	8.2^0	0.01	380
5	18.4^0	3.1^0	35^0	8.4^0	0.01	390

workpiece. As a result, reduces the strain hardening in the broached workpiece. Also, by increasing α_0 (angle of the second tooth chip) from 35 degrees to 45 degrees, the maximum micro hardness created in the workpiece has increased from 383 Vickers to 401 Vickers. Increasing α_0 increases the cutting force. As a result, strain hardening in the broached workpiece increased.

Moreover, by increasing β_0 (clearance angle of the second tooth) from 8.4 degrees to 9 degrees, the maximum micro hardness created in the workpiece decreased from 390 Vickers to 383 Vickers. Increasing β_0 reduces the contact of the tool with the workpiece surface. As a result, the strain hardening in the broached workpiece decreased.

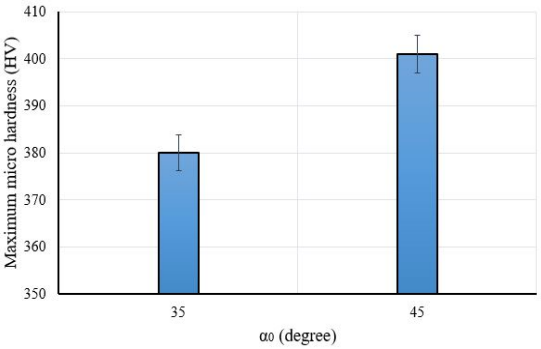

Figure 24. Effect of the rake angle (α_0) on the maximum micro hardness of broached specimens

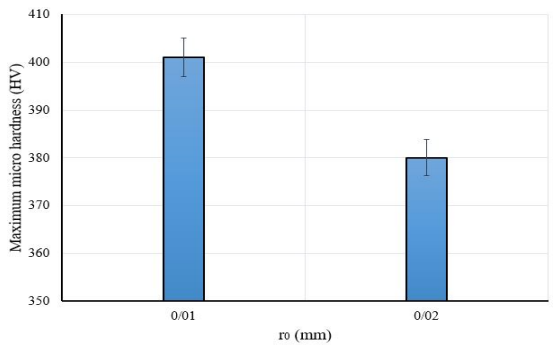

Figure 23. Effect of radius of the cutting edge (r_0) on the maximum micro hardness of broached specimens

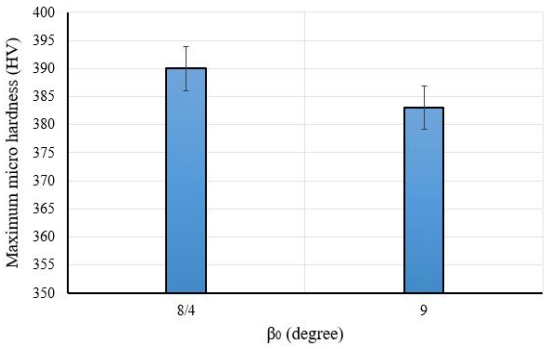

Figure 25. Effect of the clearance angle (β_0) on the maximum micro hardness of broached specimens

The results of the surface integrity investigation of broached samples are shown in Table 10. These results show that the sample broached by tool number 1(α = 18.4, β = 3.1, α_0 = 45, β_0 = 9, r_0 = 0.02) has higher surface integrity because it has the smoothest surface and the thinest deformed layer, is less thick than the other samples. Since the main criterions in selecting the optimal tool are to create the smoothest surface and the least deformed layer depth in the broached sample, tool number 1(α = 18.4, β = 3.1, α_0 = 45, β_0 = 9, r_0 = 0.02) is suggested as the optimal tool.

TABLE 10. Results of the surface integrity investigation of broached samples

Tool's No.	Ra (µm)	Rz (µm)	Residual stress (MPa)	Depth of deformed layer (µm)	Maximum micro hardness (HV)
1	0.162	0.316	205	65	380
2	0.232	0.330	482	110	401
3	0.253	0.350	261	80	383
4	0.342	0.387	202	65	380
5	0.216	0.324	367	95	390

4. CONCLUSION

This study investigates the surface integrity of Ti6Al4V by broaching. The different surface integrity aspects including: surface roughness, residual stress, microstructural, and micro hardness, are investigated.

- The results of measuring the surface roughness of the broached specimens indicate that an increase in r_0 (radius of the cutting edge of the second tooth) from 0.01 mm to 0.02 mm, decrease the R_a and R_z of the broached surface from 0.232 µm and 0.330 µm to 0.162 µm and 0.316 µm, respectively. Increasing the radius of the cutting edge reduces the penetration of the tool into the workpiece. As a result, reduces the residual stress created in broached surface. Also, with increasing α_0 (rake angle of the second tooth) from 35 degrees to 45 degrees, the R_a and R_z of the broached surface decrease from 0.253 µm and 0.350 µm to 0.232 µm and 0.336 µm, respectively. Increasing α_0 reduces the thrust force and as a result, the surface roughness is decreased. Moreover, with increasing β_0 (clearance angle of the second tooth) from 8.4 degrees to 9 degrees, the R_a and R_z of the broached surface increase from 0.216 µm and 0.324 µm to 0.253 µm and 0.350 µm, respectively. Increasing β_0 reduces the contact of the tool with the workpiece surface. As a result, the surface roughness increased.
- The results of measuring the residual stress of the broached specimens indicate that increasing r_0 (radius of the cutting edge of the second tooth) from 0.01 mm to 0.02 mm, causes a considerable decrease in the compressive residual stress created in the work piece from 482 MPa to 205 MPa. Increasing the radius of the cutting edge reduces the penetration of the tool into the work piece. As a result, reduces the residual stress created in broached surface. Also, with increasing α_0 (rake angle of the second tooth) from 35 degrees to 45 degrees, the compressive residual stress created in the work piece increases from 261 MPa to 482 MPa. Increasing α_0 increases the cutting force. As a result, the residual stress created in broached surface is increased. Moreover, with increasing β_0 (clearance angle of the second tooth) from 8.4 degrees to 9 degrees, compressive residual stress created in the work piece decreases from 367 MPa to 261 MPa. Increasing β_0 reduces the contact of the tool with the work piece surface. As a result, the residual stress created in broached surface decreased.
- The results of microstructural images of the broached specimens show that increasing r_0 (radius of the cutting edge of the second tooth) from 0.01 mm to 0.02 mm, causes a considerable decrease in the depth of the deformed layer in the broached specimen from 110 µm to 65 µm. Increasing the radius of the cutting edge reduces the penetration of the tool into the work piece. As a result, reduces the depth of the deformed layer. Also, with increasing α_0 (rake angle of the second tooth) from 35 degrees to 45 degrees, the depth of the deformed layer in the broached sample increases from 80 µm to 110 µm. Increasing α_0 increases the cutting force. As a result, the depth of the deformed layer is increased. Moreover, by increasing β_0 (clearance angle of the second tooth) from 8.4 degrees to 9 degrees, the depth of the deformed layer in the broached sample decreases from 95 µm to 80 µm. Increasing β_0 reduces the contact of the tool with the workpiece surface. As a result, the depth of deformed in workpiece decreased.
- The micro hardness measurements results of the broached workpieces show that increasing r_0 (radius of the cutting edge of the second tooth) from 0.01 mm to 0.02 mm, decreases the maximum micro hardness created in the workpiece from 401 Vickers to 380 Vickers. Also, with increasing α_0 (rake angle of the second tooth) from 35 degrees to 45 degrees, the maximum micro hardness created in the workpiece has increased from 383 Vickers to 401 Vickers. Increasing α_0

increases the cutting force. As a result, strain hardening in the broached workpiece is increased. Moreover, by increasing β_0 (clearance angle of the second tooth) from 8.4 degrees to 9 degrees, the maximum micro hardness created in the workpiece decreases from 390 Vickers to 383 Vickers. Increasing β_0 reduces the contact of the tool with the workpiece surface. As a result, the strain hardening in the broached work piece decreased.

- These results show that the sample broached by tool number 1(α = 18.4, β = 3.1, α_0 = 45, β_0 = 9, r_0 = 0.02) has higher surface integrity because it has the smoothest surface and the thinnest deformed layer among the other samples. Since the main criterions in selecting the optimal tool are to create the smoothest surface and the least deformed layer depth in the broached sample, tool number 1(α = 18.4, β = 3.1, α_0 = 45, β_0 = 9, r_0 = 0.02) is suggested as the optimal tool.

5. REFERENCES

1. DeGarmo, E., Black, J., and Kohser, R. DeGarmo's materials and processes in manufacturing. John Wiley & Sons.
2. Bordin, A., Sartori, S., Bruschi, S., and Ghiotti, A. "Experimental investigation on the feasibility of dry and cryogenic machining as sustainable strategies when turning Ti6Al4V produced by Additive Manufacturing." ***Journal of Cleaner Production***, Vol. 142, (2017), 4142–4151. https://doi.org/10.1016/j.jclepro.2016.09.209
3. Bruschi, S., Bertolini, R., Bordin, A., Medea, F., and Ghiotti, A. "Influence of the machining parameters and cooling strategies on the wear behavior of wrought and additive manufactured Ti6Al4V for biomedical applications." ***Tribology International***, Vol. 102, (2016), 133–142. https://doi.org/10.1016/j.triboint.2016.05.036
4. Davim, J. P. Machining: fundamentals and recent advances. London: Springer Science & Business Media, 2008. https://doi.org/10.1007/978-1-84800-213-5
5. Davim, J. Surface integrity in machining. Springer Science & Business Media, 2010. Retrieved from https://link.springer.com/content/pdf/10.1007/978-1-84882-874-2.pdf
6. Ulutan, D., and Ozel, T. "Machining induced surface integrity in titanium and nickel alloys: A review." ***International Journal of Machine Tools and Manufacture***, Vol. 51, No. 3, (2011), 250–280. https://doi.org/10.1016/j.ijmachtools.2010.11.003
7. Novovic, D., Dewes, R. C., Aspinwall, D. K., Voice, W., and Bowen, P. "The effect of machined topography and integrity on fatigue life." ***International Journal of Machine Tools and Manufacture***, Vol. 44, No. 2–3, (2004), 125–134. https://doi.org/10.1016/j.ijmachtools.2003.10.018
8. Liao, Z., la Monaca, A., Murray, J., Speidel, A., Ushmaev, D., Clare, A., Axinte, D., and M'Saoubi, R. "Surface integrity in metal machining - Part I: Fundamentals of surface characteristics and formation mechanisms." ***International Journal of Machine Tools and Manufacture***, Vol. 162, (2021), 103687. https://doi.org/10.1016/j.ijmachtools.2020.103687
9. He, G., and Zhang, Y. Z. "Experimental Investigations of the Surface Integrity of Broached Titanium Alloy." ***CIRP Annals***, Vol. 34, No. 1, (1985), 491–494. https://doi.org/10.1016/S0007-8506(07)61818-6
10. Schulze, V., Osterried, J., and Strauß, T. "FE analysis on the influence of sequential cuts on component conditions for different machining strategies." ***Procedia Engineering***, Vol. 19, (2011), 318–323. https://doi.org/10.1016/j.proeng.2011.11.119
11. Kong, X., Li, B., Jin, Z., and Geng, W. "Broaching Performance of Superalloy GH4169 Based on FEM." ***Journal of Materials Science & Technology***, Vol. 27, No. 12, (2011), 1178–1184. https://doi.org/10.1016/S1005-0302(12)60015-2
12. Jafarian, F., Amirabadi, H., and Fattahi, M. "Improving surface integrity in finish machining of Inconel 718 alloy using intelligent systems." ***The International Journal of Advanced Manufacturing Technology***, Vol. 71, No. 5–8, (2014), 817–827. https://doi.org/10.1007/s00170-013-5528-2
13. Jafarian, F., Amirabadi, H., and Sadri, J. "Experimental measurement and optimization of tensile residual stress in turning process of Inconel718 superalloy." ***Measurement***, Vol. 63, , (2015), 1–10. https://doi.org/10.1016/j.measurement.2014.11.021
14. Ortiz-de-Zarate, G., Madariaga, A., Garay, A., Azpitarte, L., Sacristan, I., Cuesta, M., and Arrazola, P. J. "Experimental and FEM analysis of surface integrity when broaching Ti64." ***Procedia CIRP***, Vol. 71, (2018), 466–471. https://doi.org/10.1016/j.procir.2018.05.033
15. Kaway, P. K., and Zhang, X. "Experimental Study on Surface Integrity of Titanium Alloy Ti6Al4V by Ball End Milling" ***Journal of the Institute of Engineering***, Vol. 14, No. 1, (2018), 115–121. https://doi.org/10.3126/jie.v14i1.20074
16. Childs, T. H. C., Arrazola, P.-J., Aristimuno, P., Garay, A., and Sacristan, I. "Ti6Al4V metal cutting chip formation experiments and modelling over a wide range of cutting speeds." ***Journal of Materials Processing Technology***, Vol. 255, (2018), 898–913. https://doi.org/10.1016/j.jmatprotec.2018.01.026
17. Bertolini, R., Lizzul, L., Bruschi, S., and Ghiotti, A. "On the surface integrity of Electron Beam Melted Ti6Al4V after machining." ***Procedia CIRP***, Vol. 82, (2019), 326–331. https://doi.org/10.1016/j.procir.2019.04.166
18. Khanjanzadeh, P., Amirabadi, H., and Sadri, J. "Design of Broaching Tool Using Finite Element Method for Achieving the Lowest Residual Tensile Stress in Machining of Ti6Al4V Alloy." ***International Journal of Engineering, Transaction A: Basics***, Vol. 33, No. 4, (2020), 557–567. https://doi.org/10.5829/ije.2020.33.04a.17
19. Lampman, S. "Wrought Titanium and Titanium Alloys." In Properties and Selection: Nonferrous Alloys and Special-Purpose Materials (pp. 592–633). ASM International. https://doi.org/10.31399/asm.hb.v02.a0001081
20. Groover, M. Fundamentals of modern manufacturing: materials, processes, and systems. John Wiley & Song.

Persian Abstract

چکیده

کارآیی بسیاری از قطعات هواپیما، موتور فضاپیما و ایمپلنت های پزشکی به شدت با عمر خستگی آنها مرتبط بوده و بالطبع به وضعیت یکپارچگی سطح آنها، بستگی دارد. پارامترهای هندسی ابزار خانکشی تاثیر زیادی بر یکپارچگی سطح آلیاژ Ti6Al4V خانکشی‌شده دارند. این تحقیق، یکپارچگی سطح آلیاژ Ti6Al4V خانکشی‌شده را مورد مطالعه قرار داده است. تاثیر پارامترهای هندسی ابزار شامل زاویه براده (α و α_0) ، زاویه آزاد (β و β_0) و شعاع نوک ابزار (r_0) در دو دندانه انتهایی ابزار خانکشی که براده برداری را انجام می‌دهند، بر روی یکپارچگی سطح آلیاژ Ti6Al4V خانکشی‌شده به طور تجربی، مورد بررسی واقع شده است. یکپارچگی سطح خانکشی‌شده در موارد صافی سطح، تنش باقیمانده، ریزساختار و میکروسختی، بررسی و ارزیابی شده است. مجموعه نتایج بدست‌آمده نشان می‌دهد که نمونه خانکشی‌شده توسط ابزار شمار ۱ ($\alpha = 18.4°, \beta = 3.1°, \alpha_0 = 45°, \beta_0 = 9°, r_0 = 0.02mm$)، به دلیل دارا بودن صافترین سطح و کمترین لایه تغییر فرم یافته در بین نمونه‌های آزمایشی، از مناسب‌ترین یکپارچگی سطح برخوردار است. از آنجا که معیارهای اصلی در انتخاب ابزار بهینه، ایجاد صافترین سطح و کمترین ضخامت لایه تغییر فرم یافته در نمونه خانکشی‌شده می‌باشد، ابزار شماره ۱ ($\alpha = 18.4°, \beta = 3.1°, \alpha_0 = 45°, \beta_0 = 9°, r_0 = 0.02mm$) به عنوان ابزار بهینه پیشنهاد شده است.